An X-ray Timing Analysis of NGC 6814

by

Thomas Hodd

A THESIS SUBMITTED IN PARTIAL FULFILMENT OF
THE REQUIREMENTS FOR THE DEGREE OF

BACHELOR OF SCIENCE

in

Honours Astrophysics

(Department of Astronomy and Physics, Dr. Luigi C. Gallo supervising faculty)

.....
.....
.....
.....
.....

SAINT MARY'S UNIVERSITY

April 20, 2024

Abstract

X-ray Timing Analysis of NGC 6814

by *Thomas Hodd*

submitted on April 20, 2024:

We perform an X-ray timing analysis of the type 1.5 Seyfert galaxy NGC 6814 to characterise its variability as a means of understanding the structure and properties of its active galactic nucleus (AGN). Using data from five observations by the XMM-Newton and NuSTAR observatories, we employ a number of X-ray timing analysis techniques to investigate the relationships between the different components of the AGN. We find that variability in NGC 6814 during the 2016 eclipse was dominated by changes in the absorption, and that at all other epochs behaviour was similar to that of normal AGN. Our analysis of hardness ratio against flux confirms that NGC 6814 follows the "softer when brighter" trend observed in other AGN, and, from the fractional variabilities, the amplitude of these variations is found to decrease with increasing energy. No significant frequency or energy dependent lags are detected in any of the observations, indicating that the inner-disc blurred reflection component is quite weak in this source. We discuss the implications of these findings and how they support previous works that suggest a compact source of high-energy X-rays and the possibility of a non-standard accretion disc.

Contents

List of Figures

List of Tables

Chapter 1

Introduction

1.1 Active Galactic Nuclei

1.1.1 Background

Supermassive black holes (SMBHs) are found at the centres of many galaxies including our own and some of them are active, meaning they interact with their surroundings which results in high variability over observable timescales and emission of radiation across the entire electromagnetic spectrum. Galaxies that are home to an active SMBH are called active galaxies, and their SMBH and accretion disc is the central engine of an active galactic nucleus (AGN) (Carroll and Ostlie, 2017). AGN are distant and comparatively small compared to the entire host galaxy. The SMBH has a mass only around 0.3% of the stellar mass in the galaxy (Jones et al., 2015). They are unresolvable and indirect methods of observation are required to determine their structure (Gallo, 2011).

AGN are complex regions where the viewing angle through an obscuring torus results in differences in the appearance of their spectra. If viewed face-on, we observe both narrow (with widths of $\approx 400\,\mathrm{km\,s^{-1}}$) and broad (widths of $\approx 10\,000\,\mathrm{km\,s^{-1}}$) emission lines, and the galaxy is classed as a Type I Seyfert galaxy. If viewed side-on

through the torus only narrow emission lines are observed and the galaxy is classed as a Type II Seyfert (See Fig 1.1) (Jones et al., 2015). For intermediate viewing angles Types 1.2, 1.5, 1.8, are used to describe the galaxy. These AGN have spectra in between that of Types I and II, displaying some broad emission lines that are weaker than Type I.

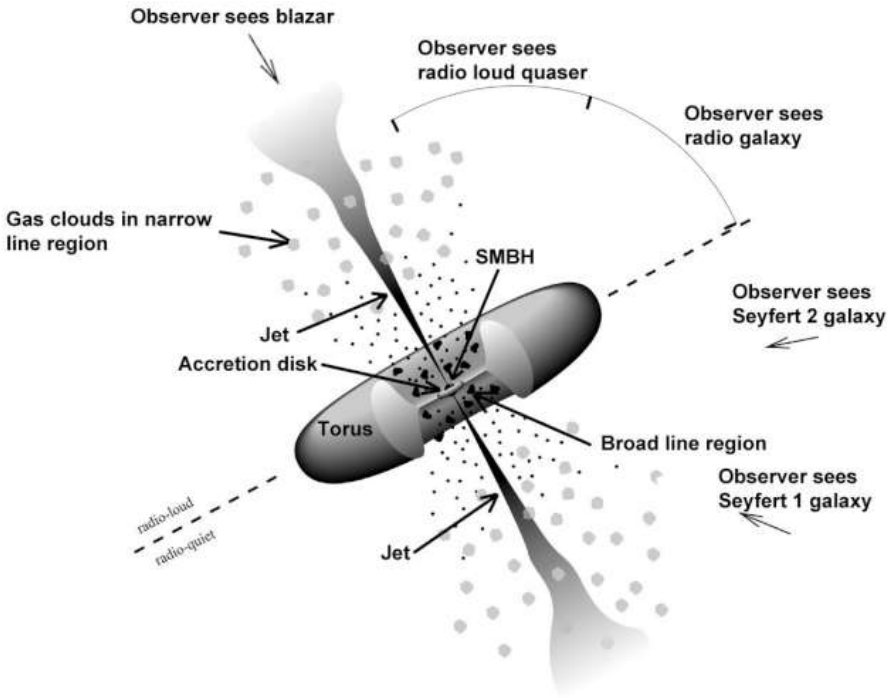

Figure 1.1: The Unification Model of AGN (Horvath, 2022). Different viewing angles relative to the obscuring torus results in different manifestations of the AGN.

1.1.2 Accretion Disc & Corona

Gas and dust surrounding the black hole fall inwards to form the accretion disc. The friction between particles in the rapidly rotating disc releases a large amount of radiation in a highly efficient process as angular momentum is lost. Theoretically, up to 42.3% of the mass can be converted to radiation (Carroll and Ostlie, 2017).

Photons emitted by the accretion disc travel to the corona, an atmosphere of hot, relativistic electrons surrounding the central engine, where collisions with electrons up-scatter the photons to X-ray energies. This process, called Comptonisation, results in a power law spectrum in the X-ray band that is referred to as the primary emission (Fig 1.2).

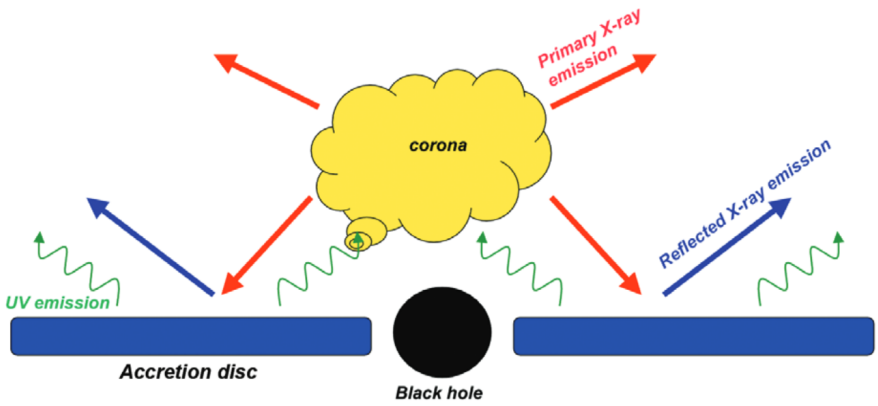

Figure 1.2: The X-ray emitting inner region of an AGN (Gallo, 2011).

Some of the X-rays emitted by the corona shine on the accretion disc where they ionise atoms. Heavier atoms will then emit photons through fluorescence to produce the reflection spectrum, which contains information about the composition and ionisation of the inner accretion disc. Often, light bending close to the black hole results in the reflected emission dominating, as paths taken by many primary emission photons are bent back towards the accretion disc and black hole.

As the corona and the accretion disc are separated by some distance, and the reflection spectrum is driven by the primary emission, the reflected component will respond to variability in the primary emission with some delay due to the light travel time between regions (Fig 1.2).

1.1.3 Broad-Line Region & Torus

The source of optical-UV broad emission lines in AGN is the broad-line region (BLR), an area of dense, clumpy, and partially ionised gas clouds that display variability on timescales of months near the AGN central engine (Carroll and Ostlie, 2017). The lines are broadened by the high speed of material orbiting close to the SMBH.

The torus is a ring of dust particles surrounding the central engine at sufficient distance that the temperature is low enough for grains of dust to survive without being vapourised (Jones et al., 2015). The torus absorbs UV and X-ray photons and re-emits them in the IR. It is thought that all AGN have a broad-line region, but due to the viewing angle through the obscuring torus, the BLR is not visible in type II Seyfert galaxies.

1.1.4 Narrow-Line Region

The narrow-line region (NLR) lies outside the torus and has a much lower electron density than the broad-line region ($10^{10}\,\mathrm{m}^{-3}$ instead of up to $10^{16}\,\mathrm{m}^{-3}$). It is thought to be a spheroidal and clumpy distribution of clouds that is more massive and larger than the broad-line region (Carroll and Ostlie, 2017). The NLR is located beyond the gravitational potential of the black hole and its motions are driven by the smooth galactic potential.

1.2 AGN TIMING ANALYSIS TECHNIQUES

Timing analyses of AGN require the measurement of flux (counts/s) over time to form a light curve (Fig 1.3), a list of the number of counts within each time interval. From this we can use a number of different methods to probe various properties of the AGN.

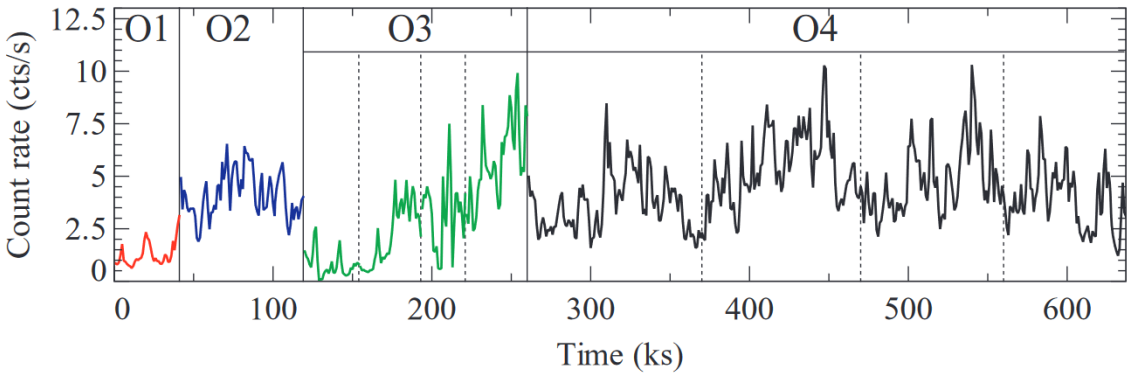

Figure 1.3: An example of the X-ray ($0.3 - 10\,\mathrm{keV}$) light curve of the AGN 1H 0707-495 taken with XMM-Newton (Zoghbi et al., 2010).

1.2.1 HARDNESS RATIO

The hardness ratio of two energy bands can be used to analyse the energy dependent variability of a source. It can be defined as:

$$HR = \frac{(H - S)}{(H + S)} \tag{1.1}$$

Where H is the count rate in the high-energy band (hard) and S is the count rate in the low-energy band (soft). The difference $(H - S)$ is normalised to the total count rate $(H + S)$ (Gonzalez et al., 2020). In our timing analysis, we bin data and calculate

the hardness ratio of each bin, against time. This can reveal changes in spectral shape as a function of time. In the X-ray, the hard band flux is typically dominated by the power law spectrum, and the soft band flux by the reflection component.

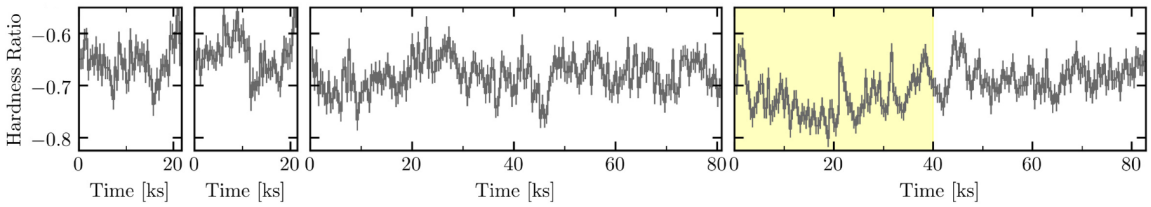

Figure 1.4: An example of hardness ratio against time, $HR = (H-S)/(H+S)$. Here the hard band is 2-10 keV and the soft band is 0.3-1 keV. From XMM-Newton observations of the AGN IRAS 17020+4544 (Gonzalez et al., 2020).

Hardness ratios are one of the components studied in Gonzalez et al. (2020), where they used it to confirm whether IRAS 17020+4544 follows the typical "softer when brighter" trend. For IRAS 17020+4544, it is found that it sometimes does not - instead tending to be harder when brighter. A number of possible reasons are given, including a variable power law or the jet emission influencing or otherwise being connected to the X-ray emission.

1.2.2 FRACTIONAL VARIABILITY

To gain some insight into the intrinsic variability of a source, we may consider the excess variance. This is the variance remaining after accounting for the errors in the measurement (Vaughan et al., 2003):

$$\sigma_{XS}^2 = S^2 - \overline{\sigma_{err}^2} \tag{1.2}$$

Here, S^2 is the variance and $\overline{\sigma_{err}^2}$ is the mean squared error. This can then be normalised by dividing by the mean square flux $\bar{x}^2$. The fractional variability is the square root of this:

$$F_{var} = \sqrt{\frac{S^2 - \overline{\sigma_{err}^2}}{\bar{x}^2}} \tag{1.3}$$

By splitting the light curve of an AGN into different energy bands we can determine whether the X-ray variability is dependent on the energy by plotting F_{var} against energy. For this to be useful we must be able to distinguish between features that result from random noise in the data and features that result from intrinsic variations of the AGN, so it is necessary to estimate the uncertainty in F_{var}. Vaughan et al. (2003) uses a Monte Carlo approach to determine the uncertainty and finds that the error due to Poisson noise to be:

$$err(F_{var}) = \sqrt{\left\{\sqrt{\frac{1}{2N}} \cdot \frac{\overline{\sigma_{err}^2}}{\bar{x}^2 F_{var}}\right\}^2 + \left\{\sqrt{\frac{\overline{\sigma_{err}^2}}{N}} \cdot \bar{x}\right\}^2} \tag{1.4}$$

With this we can determine whether the flux variability in any two simultaneously observed light curves is consistent across bands (achromatic) or not. If the difference between the two bands is significant then some of the variability results from the intrinsic properties of the source and is not entirely due to measurement errors.

Gonzalez et al. (2020), found the fractional variability in IRAS 17020+4544 to be unlike many AGN. IRAS 17020+4544 was observed to have higher fractional variability at higher energies. This was unusual as in most AGN the expected trend is a peak at lower energies or a flat curve. Combined with the "harder when brighter"

trend they found, this suggested that there was jet activity and that the power law spectral component produced by the X-ray corona might be linked to the base of the radio jet.

1.2.3 FOURIER ANALYSIS TECHNIQUES

Timing analysis of AGN in the X-ray typically uses Fourier techniques. The Fourier power spectrum easily describes the underlying structure of stochastic variable processes, where the statistical errors are nearly independent between frequency bins (Uttley et al., 2014). While Fourier techniques are difficult to apply to non-continuous datasets, they work well for the continuous and long (100 ks or more) XMM-Newton and NuSTAR observations that we will be analysing.

The starting point for the Fourier analysis methods reviewed in Uttley et al. (2014) is the power spectral density function (PSD), which describes the average variance per unit frequency of a signal at a given temporal frequency f. An estimate of the PSD can be obtained from the discrete Fourier transform (DFT) of a light curve x with fluxes binned into N contiguous time bins of widths Δt:

$$X_n = \sum_{k=0}^{N-1} x_k e^{\frac{2\pi i n k}{N}} \tag{1.5}$$

Here, x_k is the k^{th} value in the light curve. X_n is the DFT at Fourier frequency $f_n = \frac{n}{N\Delta t}$, so the minimum frequency is $1/N\Delta t$ and the maximum is the Nyquist frequency: $f_{max} = 1/2\Delta t$. From the DFT, the estimate of the PSD is given by the

periodogram of the product X_n with its complex conjugate X_n^*:

$$|X_n|^2 = X_n^* X_n \tag{1.6}$$

The periodogram can be normalised by dividing by the Nyquist frequency, the number of time bins, and the square of the mean flux $\langle x \rangle^2$:

$$|P_n| = \frac{2\Delta t}{\langle x \rangle^2 N} |X_n|^2 \tag{1.7}$$

We explore two useful applications of this technique in the following sections.

1.2.4 LAG-FREQUENCY SPECTRA

To compare two light curves at two different energy bands $x(t)$ and $y(t)$, we can calculate the Fourier cross-spectrum:

$$C_{XY,n} = X_n^* Y_n \tag{1.8}$$

Then by considering the complex polar form of the Fourier transform we can use the cross-spectrum to derive the frequency dependent lag between the two light curves (Uttley et al., 2014). This led to the discovery of soft lags and reverberation at high frequencies when Fabian et al. (2009) found that the hard band flux changes before the soft band flux in the active galaxy 1H 0707-495. By convention, positive lags indicate the hard band flux lags the soft band.

One of the first identifications of a soft lag in AGN was made by Zoghbi et al. (2010) where they used this technique to detect a soft lag in 1H0707-495 (Fig 1.5). In their analysis they found that below $5 \cdot 10^{-4}$ Hz the soft flux leads the hard by about 150 s, and that at $6 \cdot 10^{-4}$ Hz the lag becomes negative, so that the hard band is now leading. In their discussion they suggest a possible model to explain the hard lag is the propagation of accretion fluctuations. This model involves accretion rate variations that are produced at different radii in the accretion disc, and propagate inward, modulating the central X-ray emitting region. The source of the soft lag was uncertain as none of the models they discussed could accurately describe all their observations.

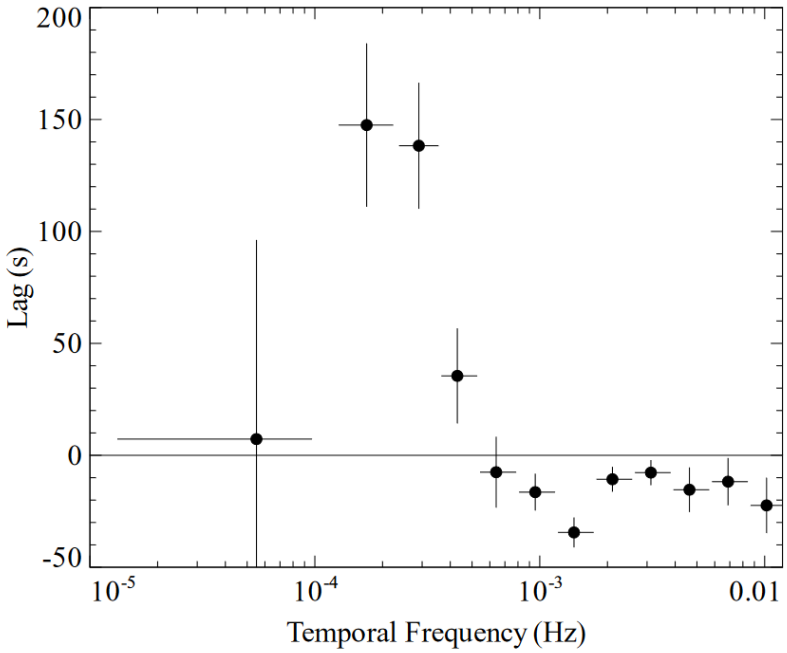

Figure 1.5: An example of a lag-frequency spectrum of the AGN 1H 070-495, showing that the hard band flux lags the soft band flux by around 150 s in the region below $2 \cdot 10^{-4}$ Hz. Above $2 \cdot 10^{-4}$ Hz, the hard band leads (Zoghbi et al., 2010).

1.2.5 Lag-Energy Spectra

Plotting a lag-energy spectrum allows for the determination of which spectral components contribute to the lags in the lag-frequency spectra (Uttley et al., 2014). To do this, we must prepare separate light curves for each energy band we want to investigate, then perform the Fourier analysis techniques discussed above for each energy band. We can then plot the lag as a function of energy, compared to some reference band, to obtain the lag-energy spectrum (Fig 1.6).

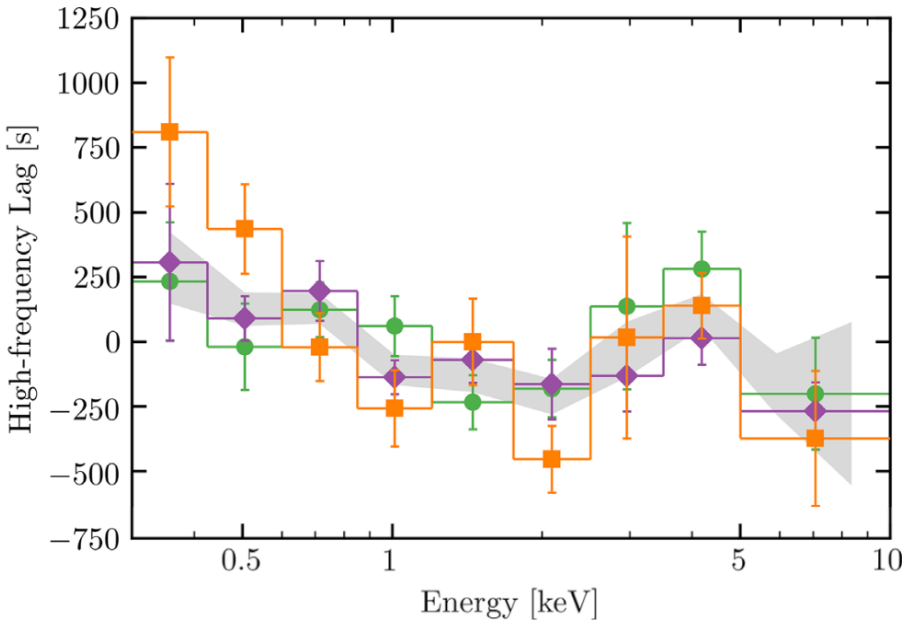

Figure 1.6: An example of a lag-energy plot for the AGN IRAS 17020+4544, showing that the lag at a given frequency is also energy dependent (Gonzalez et al., 2020).

For IRAS 17020+4544, Gonzalez et al. (2020) plot a lag-energy spectrum to search for an expected lag. The lag-energy spectrum did not show such a lag, suggesting that the emission feature was not responding to continuum variations. This could be the case if the emission region was significantly further away from the inner disc region

than their modelling suggested. When they added this distant reflection scenario into their model a significant portion of their Fe K band deviations were reduced, although a broad emission line provided a substantial statistical improvement over the distant reflection. Other possibilities put forward included ultra-fast outflows, or a more complex reflection scenario.

1.3 pyLag: An X-ray Timing Package

pyLag is an X-ray timing analysis package written in Python (Wilkins, 2022), based on the methods reviewed in Uttley et al. (2014). It provides an object-oriented approach to generating the various calculations discussed above, meaning there is a class for each type (e.g. light curve, periodogram, cross-spectrum) with docstrings explaining their use. This allows us to input our light curves into Python and easily arrive at the lag-frequency or lag-energy plots of our light curves, with the Fourier methods performed automatically, including the estimation of errors. Additionally, pyLag includes a class to calculate the fractional variability of a set of light curves.

The `LightCurve` class provides tools for reading, writing, and manipulating light curves. `LightCurve` objects have arrays containing the time points, count rate at each time, count rate errors, time between bins, and length of bins. They can be constructed by inputting the name of the FITS file to be read into a `LightCurve` object. Additionally, these objects allow for light curves to be easily added and subtracted from one another, which is useful when calculating hardness ratios.

The `LagFrequecySpectrum` class computes and stores the lag-frequency spectrum

from pairs of input light curves, which should be passed as `LightCurve` objects, with the harder bandas the first argument and the softer band as the second. The class will then automatically calculate the lag-frequency spectrum and the errors by using the `CrossSpectrum` and `Coherence` classes that perform the Fourier techniques discussed in Sections 1.2.3 and 1.2.4.

Similarly, the `LagEnergySpectrum` class computes and stores the lag-energy spectrum of an input set of light curves within a specified frequency range. A reference band is constructed by summing all the energy bands. It then calculates the lag-energy spectrum and errors using the `CrossSpectrum` and `Coherence` classes.

The `Plot` class generates plots using the Matplotlib library (Hunter, 2007). This can be done automatically if the input is a compatible pyLag class such as `LagFrequecySpectrum` or `LagEnergySpectrum`, or manually by supplying arrays of x values, y values, their errors, and labels. Plots can be scaled and customised using various Matplotlib functions, and saved to a file.

1.4 NGC 6814

NGC 6814 is a Seyfert 1.5 grand-design spiral galaxy about 22 Mpc (z=0.00521) from Earth in Aquila, and it is characterised by moderate absorption in its X-ray spectrum (Walton et al. 2013, Gallo et al. 2021). NGC 6814 exhibits X-ray variability on time scales of hours (Walton et al., 2013) and on longer time scales of years (Mukai et al., 2003). The central black hole has a mass of about $1.4 \cdot 10^7\,\mathrm{M}_\odot$ (Bentz and Katz, 2015).

XMM-Newton took long observations of NGC 6814 in 2016 and 2021. The 2016 observation shows a distinct eclipse beginning 55 ks into the observation (Fig 1.7), with symmetric ingress and egress (Gallo et al., 2021). This eclipse was used to find the properties of the cloud of gas that caused it. By estimating the electron densities, distance and velocity, Gallo et al. (2021) found that the cloud was in the broad-line region. Furthermore, comparing the duration of ingress with the duration of the low-flux interval provided an estimate on the size of the X-ray source ($\sim 25\, r_g$).

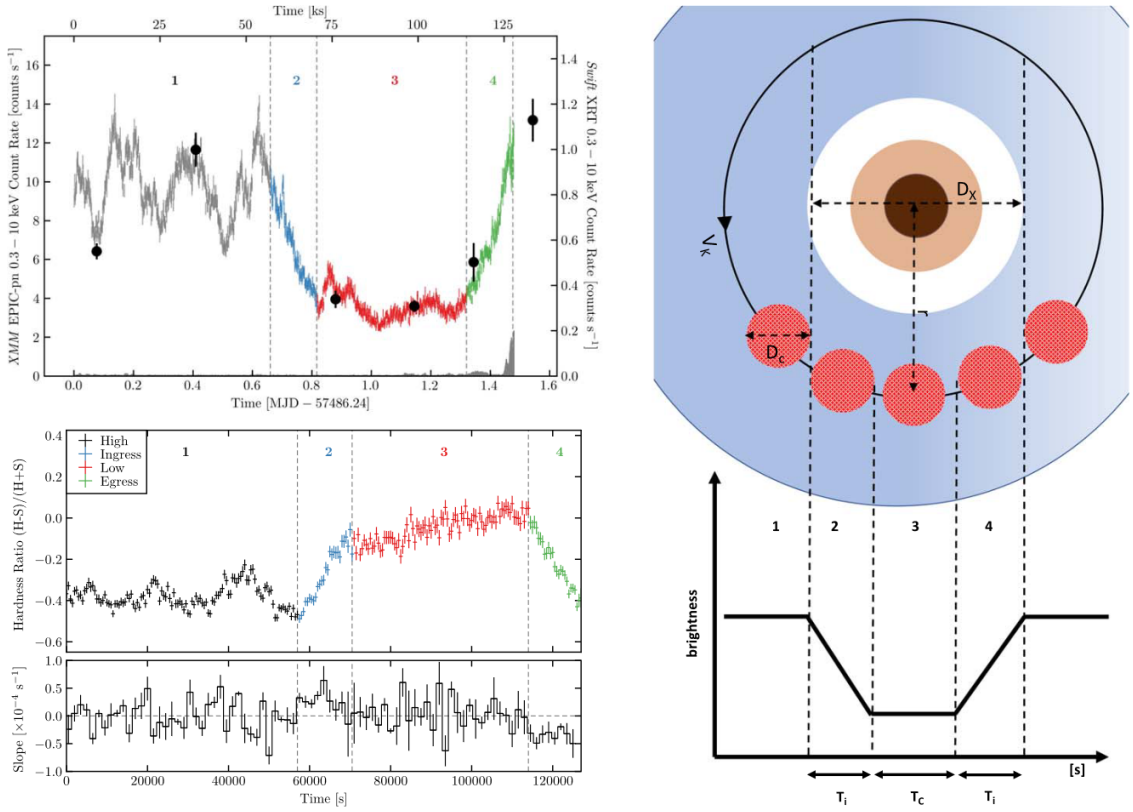

Figure 1.7: The 2016 XMM-Newton observation of NGC 6814. Upper left: Light curve recorded by XMM-Newton, showing the eclipse. Lower left: Hardness ratio curve shows hardening during the eclipse. Right: Diagram of a generic transient eclipse of the X-ray region in an AGN. (Gallo et al., 2021).

This work was followed up by Pottie et al. (2023), which performed a colour-colour analysis to investigate the changes in physical parameters during the eclipse. They found that there were changes in both covering fraction and column density. These variations proved to be inconsistent with a single, homogenous cloud, suggesting that the eclipse was caused by the combined movements of multiple individual clouds.

Gonzalez et al. (2024) presented the results of a multi-wavelength study of NGC 6814 through the X-ray, UV, and optical wavebands through a Swift monitoring campaign. They used structure function analysis to determine the X-ray and UV/optical power laws, finding the X-ray to be much flatter, suggesting different physical mechanisms drive the variability in each emission region. This leads to the possibility that NGC 6814 may have a non-standard accretion disc, which they plan to explore in future work.

1.5 Motivation

In this project we will be performing an X-ray timing analysis of NGC 6814 using a number of different techniques and simultaneous data from XMM-Newton and NuSTAR telescopes. Firstly, by studying the hardness ratios we will observe whether NGC 6814 follows the "softer when brighter" trend seen in AGN. Secondly, we will determine how the fractional variability varies depending on the energy band to see if it peaks at the low energies, is flat, or something else. Then we shall use the discussed Fourier analysis methods to search for and investigate any lags between the soft and hard energy bands. This will allow us to explore the interaction between the X-ray

emitting regions of the accretion disc and the corona in NGC 6814 and to identify any unusual behaviours or properties that require further explanation. This will help further our understanding of the nature and structure of NGC 6814.

Chapter 2

OBSERVATIONS

In our analysis we used data from the XMM-Newton (Jansen et al., 2001) and NuSTAR (Harrison et al., 2013) X-ray observatories. NGC 6814 was observed by XMM-Newton for ∼30 ks in 2009 and ∼130 ks in 2016 and 2021 (Table 2.1). These

Observation	Start date (YYYY/MM/DD)	Duration (ks)	Exposure (ks)	Energy Range (keV)
XMM 2009	2009/04/22	30	26	0.3-10
XMM 2016	2016/04/08	128	118	0.3-10
XMM 2021	2021/10/01	122	113	0.3-10
NuSTAR 2016	2016/07/04	305	148	4-50
NuSTAR 2021	2021/10/01	270	128	4-50

Table 2.1: List of observations used for our X-ray timing analysis.

observations were in the 0.3-10 keV band, and were taken with the EPIC-pn detector (Strüder et al., 2001) operating in large window mode with the medium filter. The observed light curves were split into three broad energy bands: Soft (0.3-1 keV), Mid (1-4 keV), Hard (4-10 keV), and, for 2016 and 2021, sixteen narrow energy bands. This allowed us to use either broad or narrow energy bands for different parts of our analysis depending on which type was most useful for each method. The 0.3-10 keV light curves from each of the XMM-Newton observations are shown in Fig. 2.1. The eclipse reported by Gallo et al. (2021) is present in the 2016 light curve between 50-120 ks.

NGC 6814 was also observed by NuSTAR for ∼300 ks in 2016 and ∼270 ks in 2021

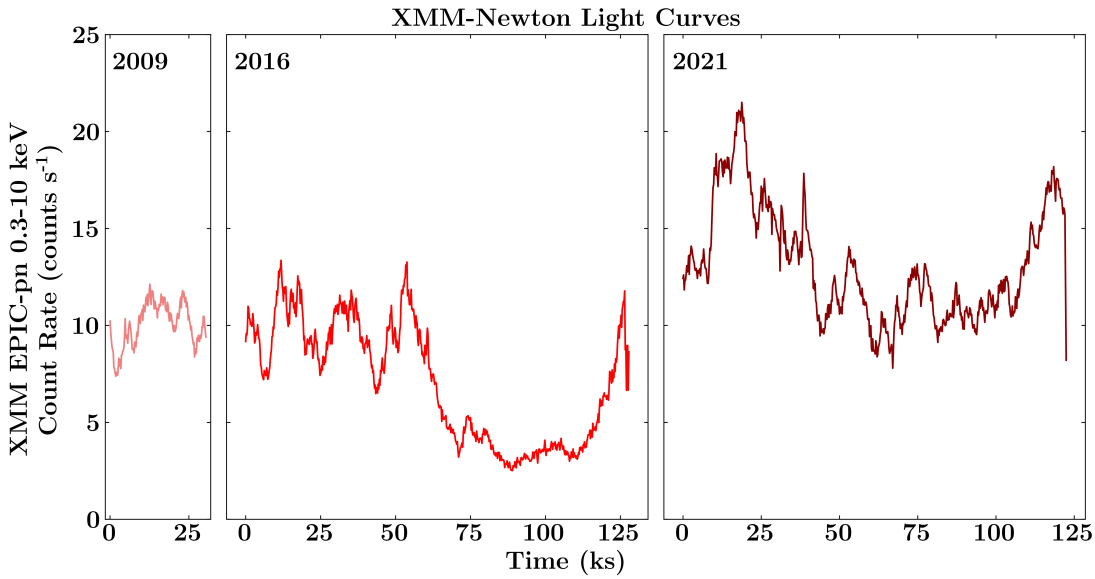

Figure 2.1: XMM-Newton EPIC-pn 0.3-10 keV light curves binned by 200 s. 2009 is in pink, 2016 is in red, and 2021 is in dark red. When the eclipse is excluded from our analysis, we take only the first 60 ks of the 2016 light curve.

(Table 2.1). During these observations both Focal Plane Modules A and B (FPMA and FPMB) were used, with data from both being combined for our analysis. Unlike the XMM-Newton observations, the NuSTAR observations are at higher energies and are not continuous. The NuSTAR light curves were split into two broad bands: Soft (4-10 keV), and Hard (10-50 keV), and in ten narrow bands (2021 only). The 4-50 keV light curves are shown in Fig. 2.2. The 2021 NuSTAR and XMM-Newton observations overlap, both starting on the same day and observing for 270 ks and 122 ks, respectively.

All the light curves were processed and background subtracted so that they could be read directly from FITS files into Python using the pyLag `LightCurve` class. These objects provide easy access to the data, as well as functions to add/subtract, rebin, replace gaps with zeroes, and split/join light curves. Light curves were edited where

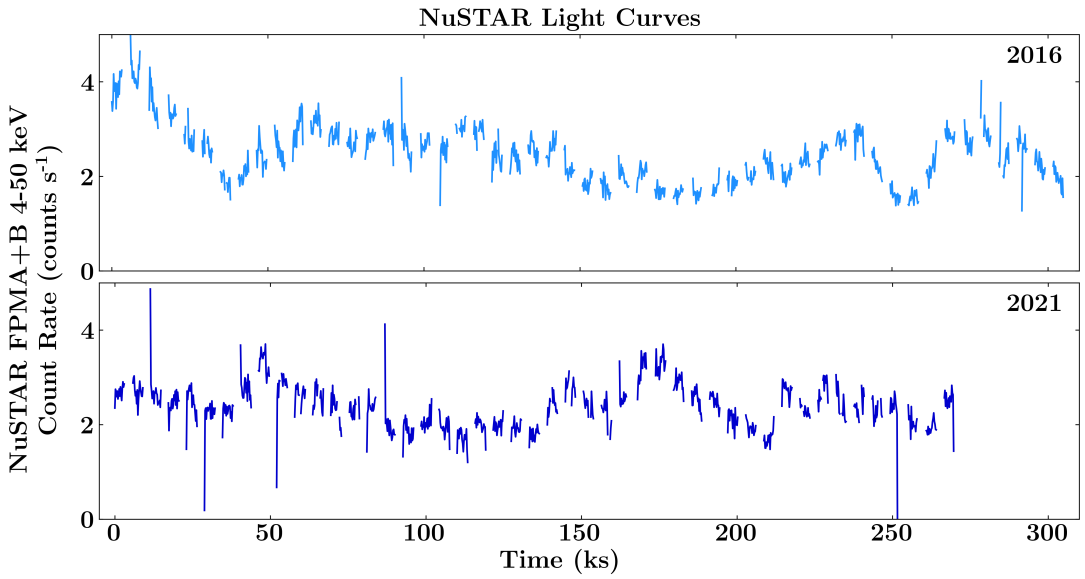

Figure 2.2: NuSTAR FPMA+FPMB 4-50 keV light curves binned by 200s. 2016 is in light blue, and 2021 is in dark blue.

necessary, for example to remove the eclipse from the 2016 data, using HEAsoft (NASA High Energy Astrophysics Science Archive Research Center (HEASARC), 2014) and viewed using the FITS viewer *fv* (Pence and Chai, 2012). Due to the differences between the telescopes, the count rates between XMM-Newton and NuSTAR are not directly comparable. By taking data from both, we can survey the widest possible range of energies in our analysis to give ourselves the best understanding of the nature of NGC 6814.

Chapter 3

Data Analysis

3.1 Hardness Ratios

To begin our analysis, we took each of the soft and hard band XMM-Newton and NuSTAR light curves, binning the data by 200 s. We then calculated the hardness ratio (Eq. 1.1) in each bin and plotted this against time (Figs. 3.1, 3.2). Both 2009

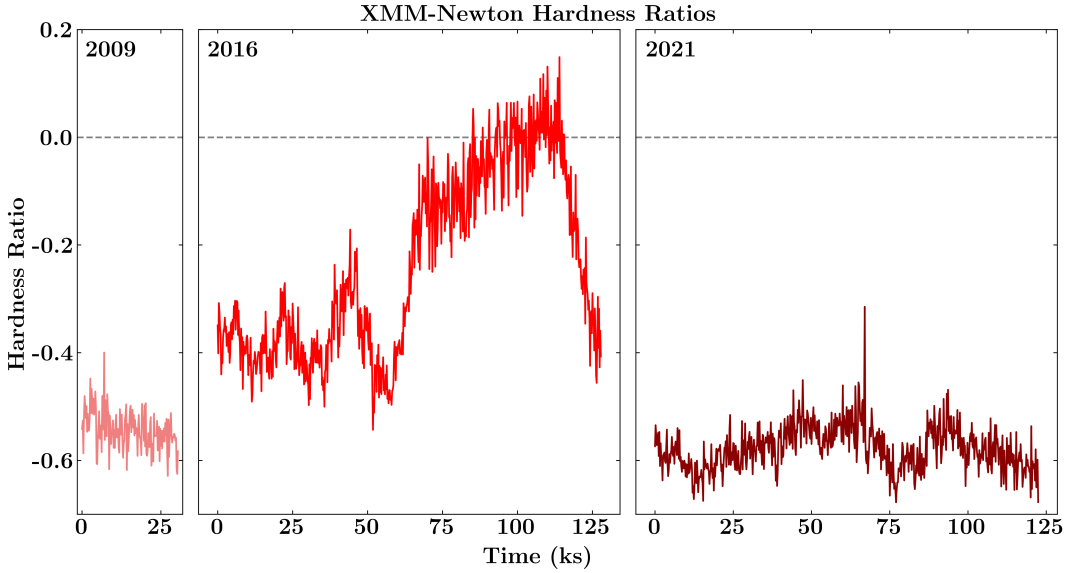

Figure 3.1: The XMM-Newton hardness ratios $(H - S)/(H + S)$ over time for each observation, binned by 200 s, where $S = 0.3 - 1\,\mathrm{keV}$, $H = 4 - 10\,\mathrm{keV}$.

and 2021 display a similar softness ($HR \approx -0.56$) in the XMM-Newton data, whilst 2016 is generally harder ($HR \approx -0.24$). This trend is matched by the NuSTAR data, although the difference between the observations is much less. The 2016 eclipse

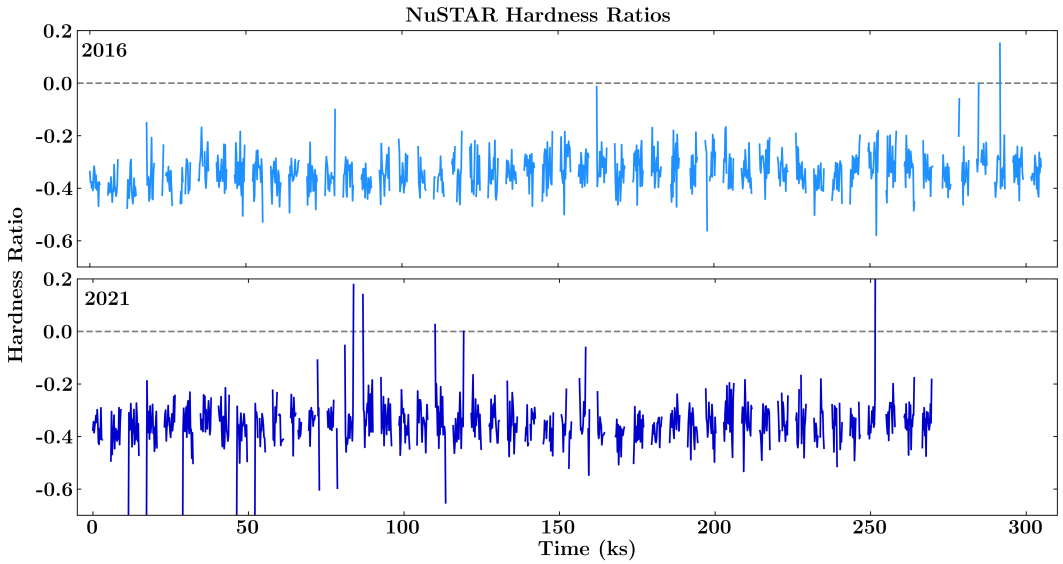

Figure 3.2: The NuSTAR hardness ratios $(H-S)/(H+S)$ over time for each observation, binned by 200 s, where $S = 4-10$ keV, $H = 10-50$ keV.

is clearly seen with a shift to a much harder ratio beginning around 60 ks into the observation. The mean count rate, mean hardness ratio, and fractional variability for each observation is given in Table. 3.1.

Observation	Mean rate (counts s^{-1})	F_{var} (%)	Mean *HR*
XMM 2009	10.05 ± 0.02	10.9 ± 0.7	-0.543 ± 0.002
XMM 2016	7.079 ± 0.008	43 ± 1	-0.239 ± 0.002
XMM 2021	13.13 ± 0.01	22.1 ± 0.6	-0.577 ± 0.001
NuSTAR 2016	2.474 ± 0.005	23.9 ± 0.6	-0.337 ± 0.002
NuSTAR 2021	2.389 ± 0.006	17.2 ± 0.6	-0.351 ± 0.002

Table 3.1: Measured light curve properties for each observation, binned by 200 s. The mean rate and F_{var} are calculated for the whole energy band, 0.3-10 keV for XMM-Newton, and 4-50 keV for NuSTAR. Mean hardness ratios are between the 0.3-1 keV and 4-10 keV bands for XMM-Newton, and between the 4-10 keV and 10-50 keV bands for NuSTAR.

The 2009 and 2021 hardness ratio curves are generally comparable with one another, whilst the 2016 XMM-Newton observation shows a distinct difference in hardness ratio in comparison to the others, even when the eclipse was off. This indicates

that there was a physical difference in the intrinsic AGN spectrum in 2016 compared to either 2009 or 2021.

The NuSTAR hardness ratios are nearly constant over both observations. This indicates that there is very little spectral variability between the bands, suggesting the 4-10 and 10-40 keV emission is likely dominated by the same spectral component (e.g. the primary continuum). We will explore the spectral variability in more detail by plotting fractional variability against energy in Section 3.2.

The softer-when-bright behaviour is often seen in accretion dominated systems. To check if our light curves follow the this trend, we plot hardness ratio against count rate (Hardness-flux), and compute the linear best-fit model for each observation (Figs. 3.3, 3.4).

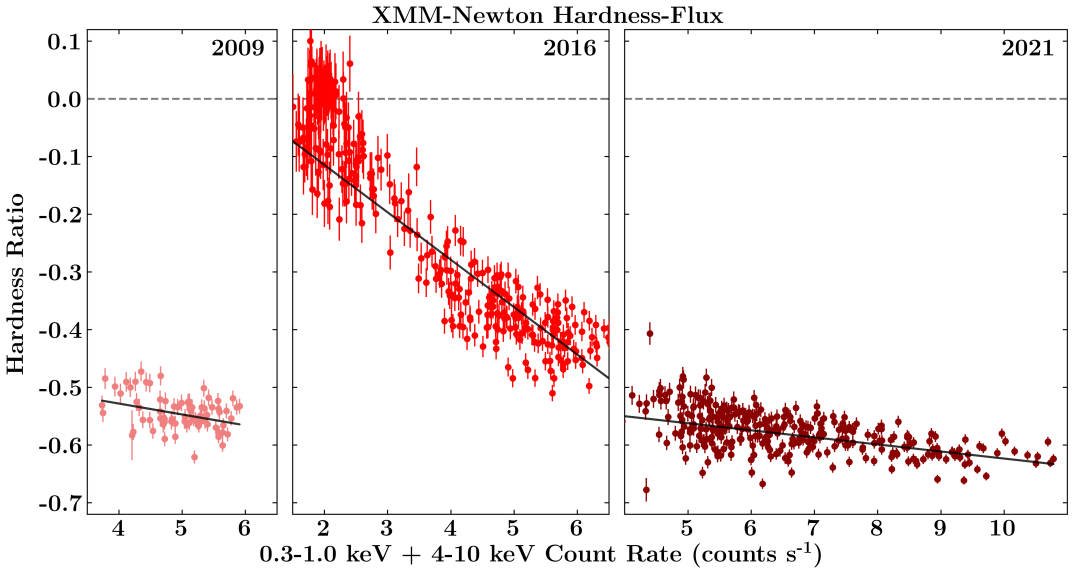

Figure 3.3: Hardness ratios against flux (Soft + Hard band counts) for the three XMM-Newton observations, light curves binned by 400 s. The solid black lines show the best-fit linear model for the hardness-flux relation.

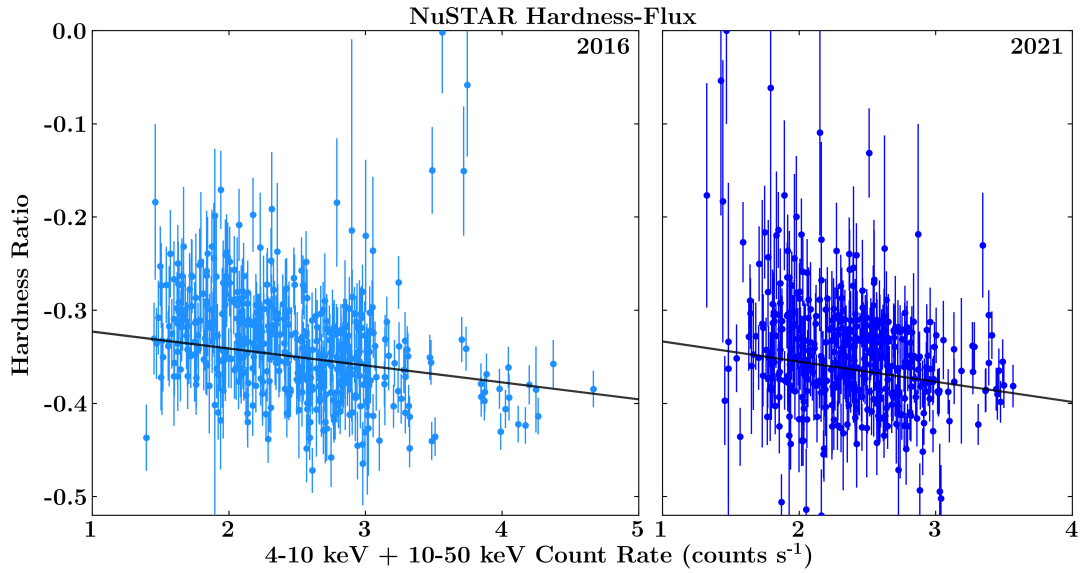

Figure 3.4: Hardness ratios against flux (Soft + Hard band counts) for the two NuSTAR observations, light curves binned by 400 s. The solid black lines show the best-fit linear model for the hardness-flux relation.

Observation	Linear best-fit model	χ^2/dof
XMM 2009	$HR = -0.02F_C - 0.5$	277/75
XMM 2016	$HR = -0.08F_C + 0.0$	1871/318
XMM 2021	$HR = -0.01F_C - 0.5$	2059/305
NuSTAR 2016	$HR = -0.02F_C - 0.3$	985/761
NuSTAR 2021	$HR = -0.02F_C - 0.3$	1621/673

Table 3.2: The linear best-fit models for the hardness-flux plots in Figs. 3.3, 3.4. The soft band (0.3-1 keV) and hard band (4-10 keV) are used, binned by 400 s. F_C is the combined flux of these two bands. The χ^2 values are given per degree of freedom (dof).

This is the same process done in Gonzalez et al. (2020). The results of the best fit models are given in Table 3.2. None of the XMM-Newton fits are statistically good, with $\chi^2/dof > 3$. Only the 2016 NuSTAR fit has $\chi^2/dof < 2$. However, we can see that the "softer when brighter" trend is followed in these observations, particularly in 2016 XMM-Newton, with higher count rates occurring with softer hardness ratios. It is interesting that 2016 XMM-Newton, with the eclipse, has a much steeper hardness-flux relationship than any of the other hardness-flux plots.

To see how the hardness of NGC 6814 has evolved over time, we created a colour-colour diagram using the three energy bands in the XMM-Newton observations. Hard colour was defined as M/H, and soft colour as S/M, with $S = 0.3 - 1\,\mathrm{keV}$, $M = 1 - 4\,\mathrm{keV}$, $H = 4 - 10\,\mathrm{keV}$. Using these colours we plot the colour-colour diagram (Fig. 3.5). Clearly NGC 6814 was in a harder state throughout the 2016 observation

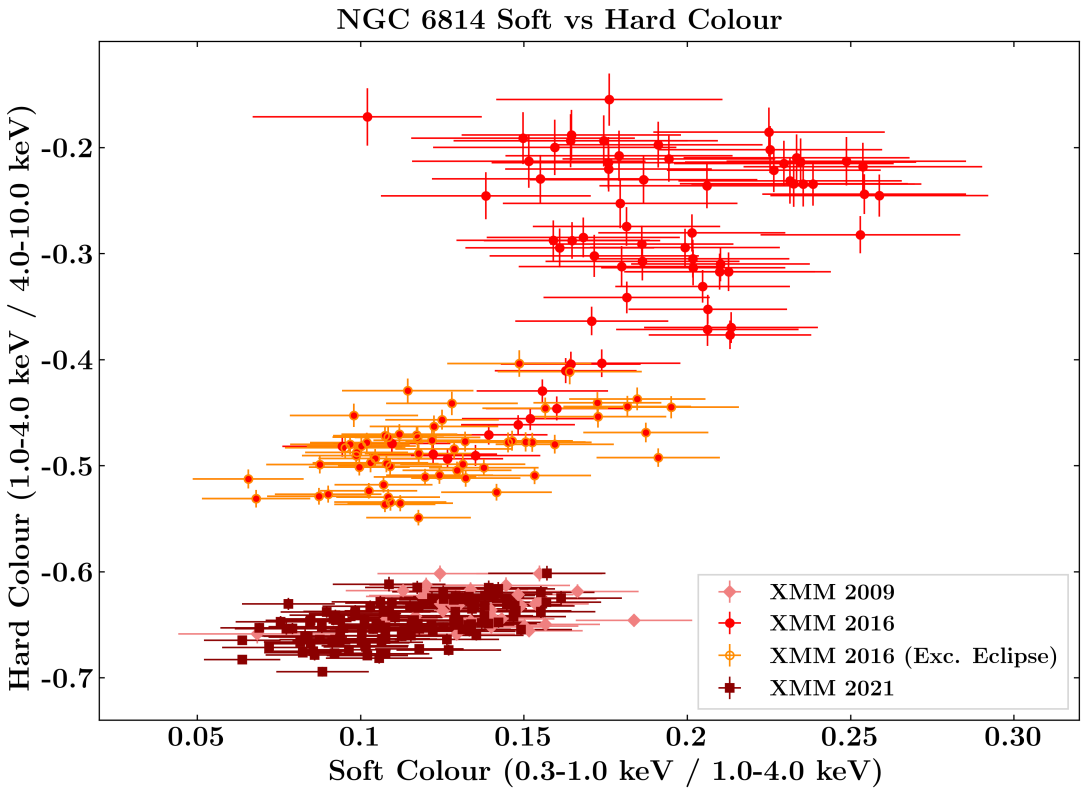

Figure 3.5: Colour-colour diagram for the XMM-Newton observations, binned by 1000 s. The 2016 (Excluding eclipse) observations, including only the first 60 ks of the 2016 observation are shown in orange.

than it was in either 2009 or 2021. Pre-eclipse the soft colour is comparable to the other observations, but the hard colour is already harder. During the eclipse, both the soft and hard colours become harder.

Our analysis so far has shown that there was significant hardening during the 2016

eclipse, and that the AGN was in a different state in that epoch. We have also found that NGC 6814 follows the "softer when brighter" trend, and that at the energies investigated by NuSTAR the spectral variability is very low.

3.2 Fractional Variability

We took a quantitative measurement of the broad band variability by calculating the fractional variability of each light curve (Vaughan et al., 2003). To do this we took all of our narrow energy band light curves and used the `fvar()` function in pyLag to calculate the fractional variability as a function of energy band midpoint. This works by evaluating Eq. 1.7 for the input `Lightcurve` objects and returning the calculated fractional variabilities and their errors. We can use this to probe the energy dependent variability of NGC 6814 in each of the observations. The narrow energy band light curves described in Chapter 2 are necessary for a more detailed analysis of the energy dependent variability than we would obtain from the two or three broad band curves used in Section 3.1.

As expected, the 2016 eclipse is significantly different and shows much more extreme variability in the soft band than any of the other observations (Fig. 3.6), although the hard band variability is not significantly different from the other observations. The 2021 observations show more variability than 2009 but still much less than 2016.

The fractional variability generally decreases with increasing energy in all the light

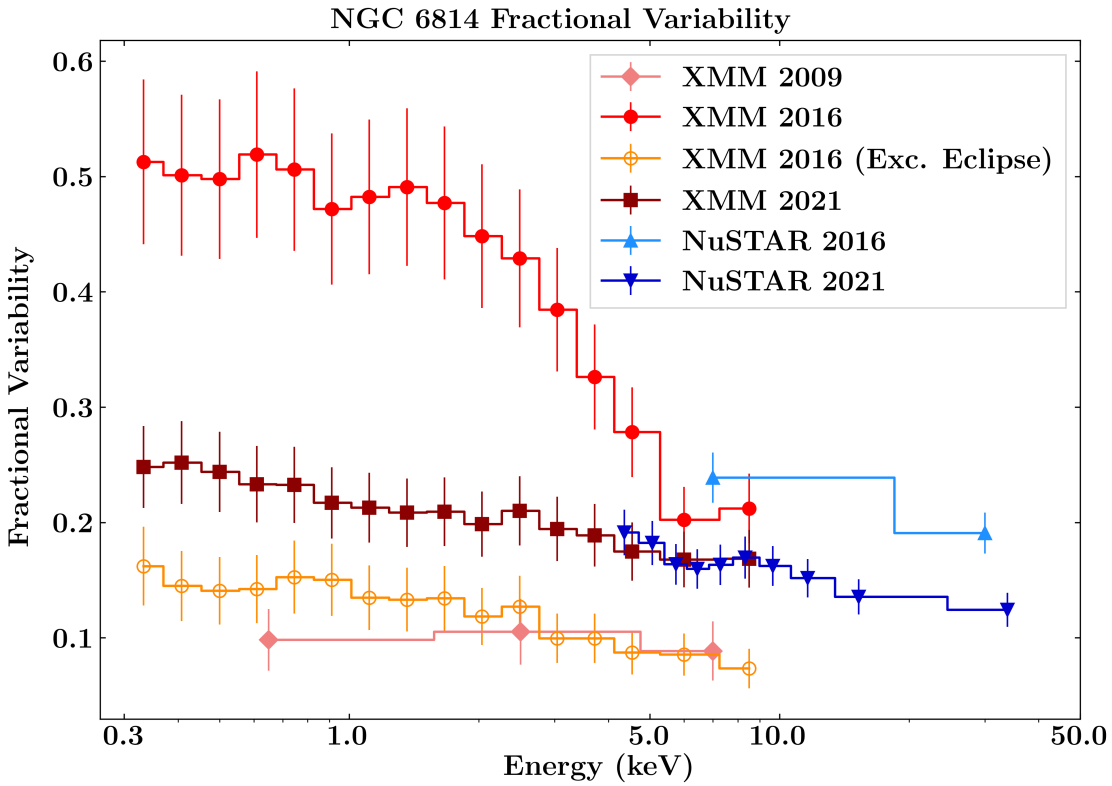

Figure 3.6: Fractional variabilities for XMM-Newton and NuSTAR light curves binned by 5 ks. The 2016 XMM-Newton observation excluding the eclipse includes only data in the first 60 ks.

curves, although this is a very weak relation and the spectral variability is mostly the same across the energies. The non-eclipse observations show similar fractional variability modified only by a normalisation constant. This suggests a similar physical state for all of the non-eclipse observations, in agreement with our hardness ratio results. The 2021 XMM-Newton and NuSTAR observations are in agreement with each other which is expected as the observations are mostly simultaneous. The 2016 NuSTAR observation shows increased variability over the 2021 observation, which matches the XMM-Newton observation, even though these observations are not simultaneous.

By investigating the fractional variability of NGC 6814 in the different observations, we have strengthened our hardness ratio findings that the AGN was in a harder and more variable state in 2016 than in 2009 or 2021. We have shown that the variability in 2021 was similar to that in 2009, so NGC 6814 has returned to a softer state from the 2016 high.

3.3 Power Spectra

The first step in performing the Fourier analysis techniques discussed in Sections 1.2.4 & 1.2.5 is to compute the power spectrum for each observation (Fig. 3.7). To do this we binned the light curves by 200 s and created a `Periodogram` with the relevant `LightCurve` object as the constructor argument. The `Periodogram` class computes (by performing a DFT on the light curve) and stores the PSD as discussed in Section 1.2.3.

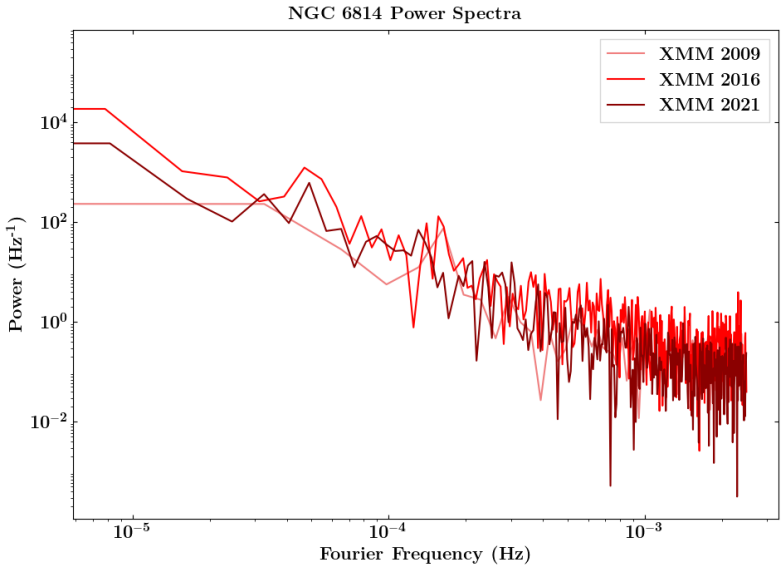

Figure 3.7: The periodogram (power spectral density) for the three XMM-Newton observations, produced with pyLag.

By plotting these objects with Fourier frequency against power we see that all the XMM-Newton observations have similar PSDs (Fig. 3.7), and that they follow an expected shape showing more power at lower frequencies. We do not observe any significant features in any of the PSDs, although further analysis is required to test if any of the peaks are of interest. The NuSTAR observations are excluded since they are not continuous and therefore not suitable for Fourier techniques. In Section 3.4.1 we will solve this problem for our lag analysis by using Gaussian processes to model the gaps in the curves. These power spectra reveal similar behaviour in NGC 6814 at the different epochs, but do not inform of any strong or obvious frequencies of interest.

3.4 Lag-Frequency

To search for a reverberation signal, we can compute the lag-frequency spectrum between pairs of our light curves, for example between the hard and soft bands of the 2021 XMM-Newton observation. pyLag provides a class for doing this, called `LagFrequencySpectrum`, which computes the lag-frequency spectrum between two input `LightCurves`. It does this by calculating the periodogram (Section 3.3), which is then used to determine the Fourier cross-spectrum and coherence between the two light curves. The result is the lag-frequency spectrum which is stored as lists of Fourier frequencies, lags, and their associated uncertainties.

To calculate the DFT, input light curves must be continuous and long. This would limit us to using only the 2016 and 2021 XMM-Newton light curves, however we can

use Gaussian processes to make our NuSTAR light curves continuous, such that they can be included in our analysis.

3.4.1 Gaussian Processes for NuSTAR Light Curves

It is necessary to model the observed NuSTAR light curves over their orbital gaps before proceeding to apply Fourier techniques to study their time variability. We can model the observed light curves as a Gaussian process and fit it to the data. This model may then be used to predict the light curve during gaps in the data.

To construct our Gaussian process model we will follow Wilkins (2019). We begin by defining two vectors: $\boldsymbol{t}$ the time of each bin, and $\boldsymbol{d}$ the data (count rate) in each bin. As we are modelling our light curve as a Gaussian process, $\boldsymbol{d}$ must be drawn from a multivariate Gaussian distribution, with the observed light curve being one possible result of this Gaussian process. If we let $\boldsymbol{x}$ be a Gaussian random vector with mean $\boldsymbol{\mu_x}$ and covariance matrix $\boldsymbol{\Sigma_{xx}}$ between element pairs in $\boldsymbol{d}$ then:

$$\boldsymbol{x} \approx \mathcal{N}(\boldsymbol{\mu_x}, \boldsymbol{\Sigma_{xx}}) \tag{3.1}$$

The likelihood function of $\boldsymbol{x}$ is:

$$p(\boldsymbol{x}|\boldsymbol{\mu_x}, \boldsymbol{\Sigma_{xx}}) = \frac{1}{(2\pi)^N |\boldsymbol{\Sigma_{xx}}|} \exp\left(-\frac{1}{2}(\boldsymbol{x} - \boldsymbol{\mu_x})^T \boldsymbol{\Sigma_{xx}^{-1}} (\boldsymbol{x} - \boldsymbol{\mu_x})\right) \tag{3.2}$$

Here, N is the number of points in our vectors $\boldsymbol{t}$ and $\boldsymbol{d}$. $\boldsymbol{\mu_x}$ can be replaced with the mean count rate as it is assumed to be constant across the observation. The covariance

matrix is determined by the kernel function, which has hyperparameters that describe the variability in the light curve. Based on Wilkins (2019), the rational quadratic kernel is best suited to our problem as it was found to work better than other kernels over longer gaps. By maximising the likelihood, we can fit these hyperparameters to our observed light curve. Once this is done, we can draw samples from our Gaussian process model over any times, including inside gaps. This means that we can use these samples to produce continuous light curves of observed data with gaps and use them in our lag analysis (Fig. 3.8).

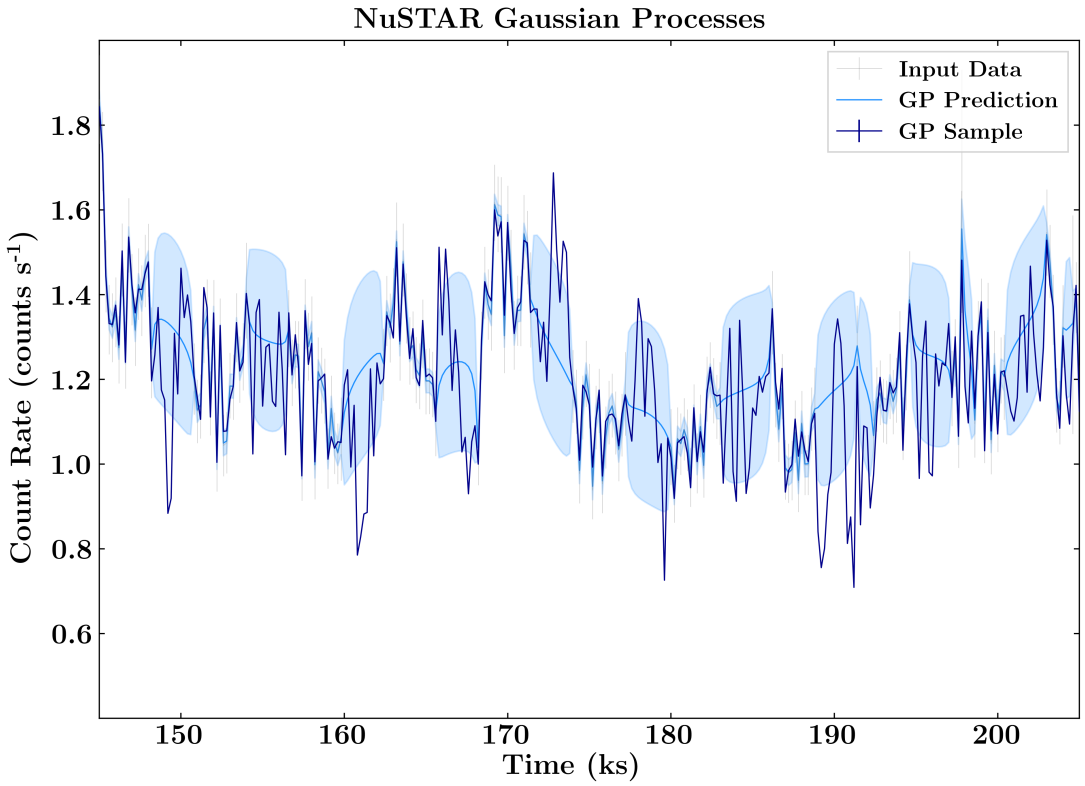

Figure 3.8: Section of NuSTAR light curve, binned by 200 s, with the Gaussian process prediction shown by the blue line and shaded region. A single sample drawn from the Gaussian process is shown in dark blue.

3.4.2 Lag-Frequency Analysis

As discussed in Section 1.2.3, the lag-frequency spectrum shows the frequency dependent lags between two light curves and may be used to infer the structure of the inner region of AGN. We computed the lag-frequency spectra of the XMM-Newton observations using the soft band (0.3-1 keV) and hard band (4-10 keV) light curves for 2016 and 2021, inputting each pair into `LagFrequencySpectrum`. The minimum and maximum (Nyquist) frequency are given in Section 1.2.3 and are about $8 \cdot 10^{-6}$ Hz and $2 \cdot 10^{-3}$ Hz, respectively, however in practice a smaller range is used as the uncertainties at the lower frequencies become very large. The XMM-Newton lag-frequency spectra are shown in Fig. 3.9.

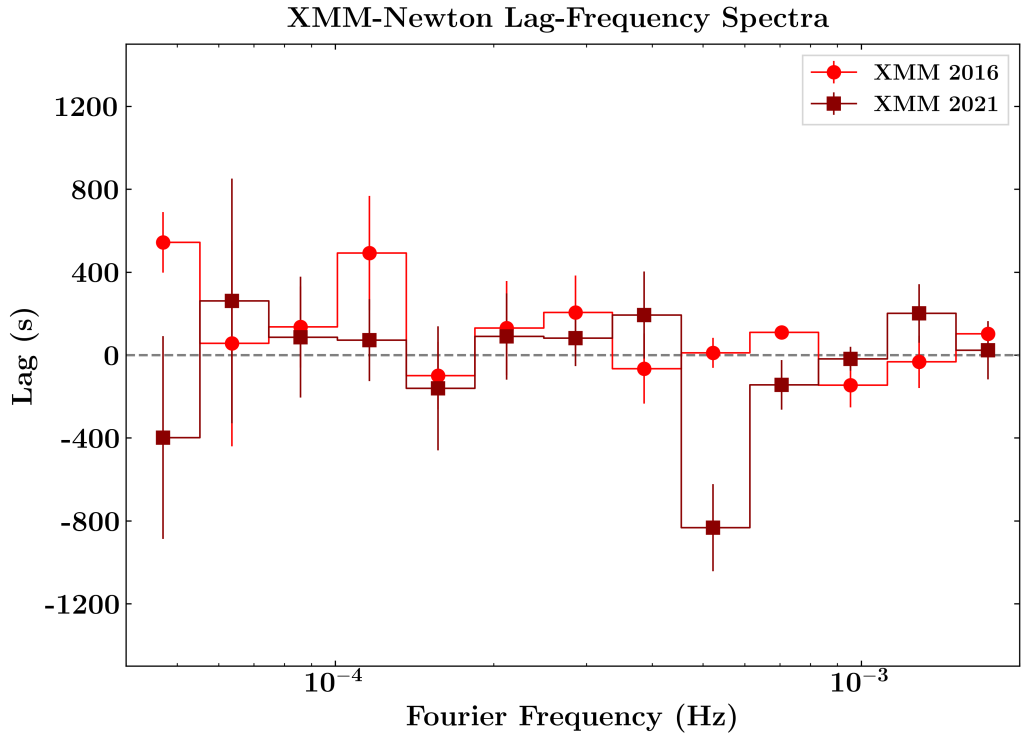

Figure 3.9: XMM-Newton lag-frequency spectra, with $f_{min} = 4 \cdot 10^{-5}$ Hz and $f_{max} = 2 \cdot 10^{-3}$ Hz, with 14 frequency bins. There is no significant lag signal.

For the NuSTAR light curves, we first construct the Gaussian process model as described above. Once this is done, we can take the desired number of samples, computing the lag-frequency spectrum of each. After this the next step is to calculate the mean lag-frequency spectrum for the observation. The results for the NuSTAR observations, in the frequency range $1 \cdot 10^{-5}$ Hz to $2 \cdot 10^{-3}$ Hz are shown in Fig. 3.10. We find that there are no significant lags in any of the spectra within this frequency range.

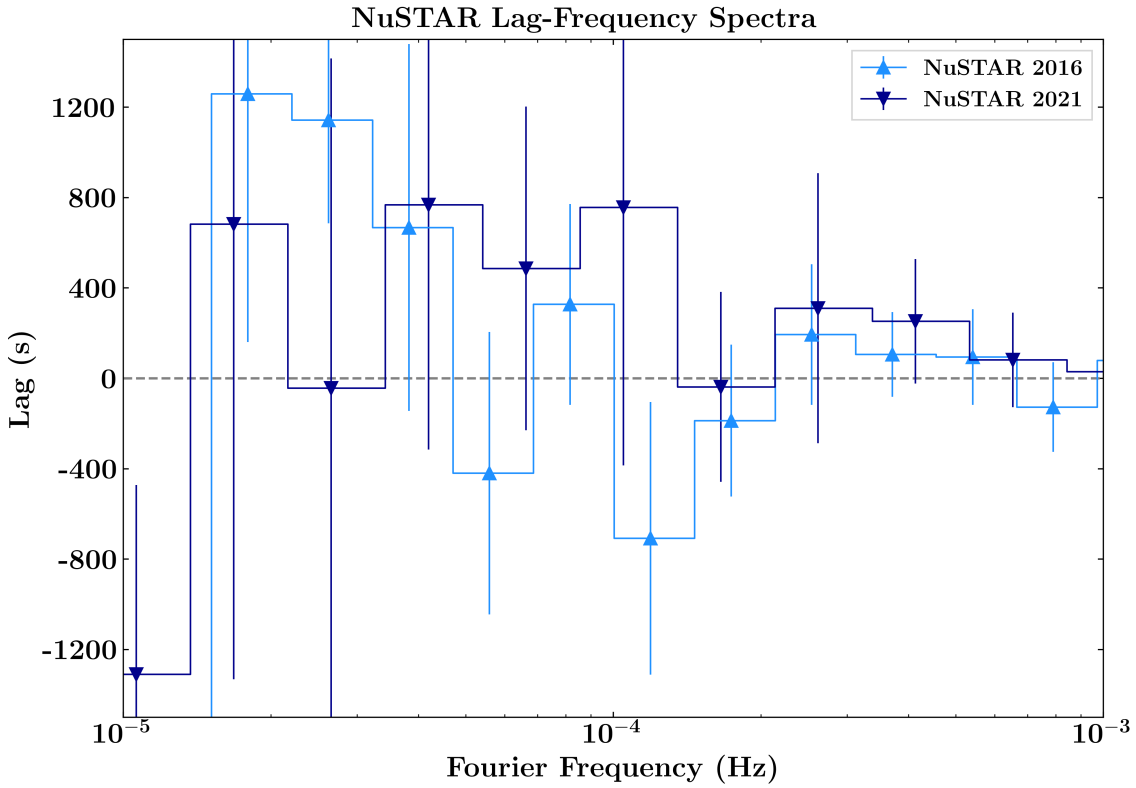

Figure 3.10: NuSTAR Lag-frequency spectra, with $f_{min} = 1 \cdot 10^{-5}$ Hz and $f_{max} = 2 \cdot 10^{-3}$ Hz, with 14 frequency bins. There is no significant lag signal.

In this section we have shown that it is possible to use Gaussian processing in order to fill the gaps in non-continuous light curves. This method allows us to apply

Fourier analysis techniques to the NuSTAR observations, providing a lag-frequency analysis in the higher energies. The fact we do not see any lags suggests that either the reflected emission is physically close to the corona, such that the primary and reflected emissions arrive at very similar times, or that the primary emission dominates the spectrum and that the reflected emission does not make up a significant number of the observed X-rays.

3.5 Lag-Energy

With the lag-frequency spectra computed, we can consider which spectral components contribute to the lag spectra by splitting our light curves into different energy bands and considering the lag in each band for a frequency region of interest. For the XMM-Newton observations we can use `LagEnergySpectrum` with the sixteen narrow bands. For the 2021 NuSTAR observation we must first compute a Gaussian process model for each of the ten narrow bands. Then we can take samples and determine the lag-energy spectrum for each one, similar to our process for the lag-frequency spectrum. Since no obvious lags were evident at any frequency in Figs. 3.9, 3.10, we select a range of interest as determined by considering the black hole mass and using the best fit relationship found by De Marco et al. (2013):

$$\log \nu_{lag} \approx -3.5 - 0.47 \log M_{BH} \tag{3.3}$$

With $M_{BH} = 1.44 \cdot 10^7$ (Bentz and Katz, 2015) we find $\nu_{lag} \approx 3 \cdot 10^{-4}$ Hz. We find that there are no significant lags in any energy in the frequency range of $2 \cdot 10^{-4} - 4 \cdot 10^{-4}$ Hz (Fig. 3.11).

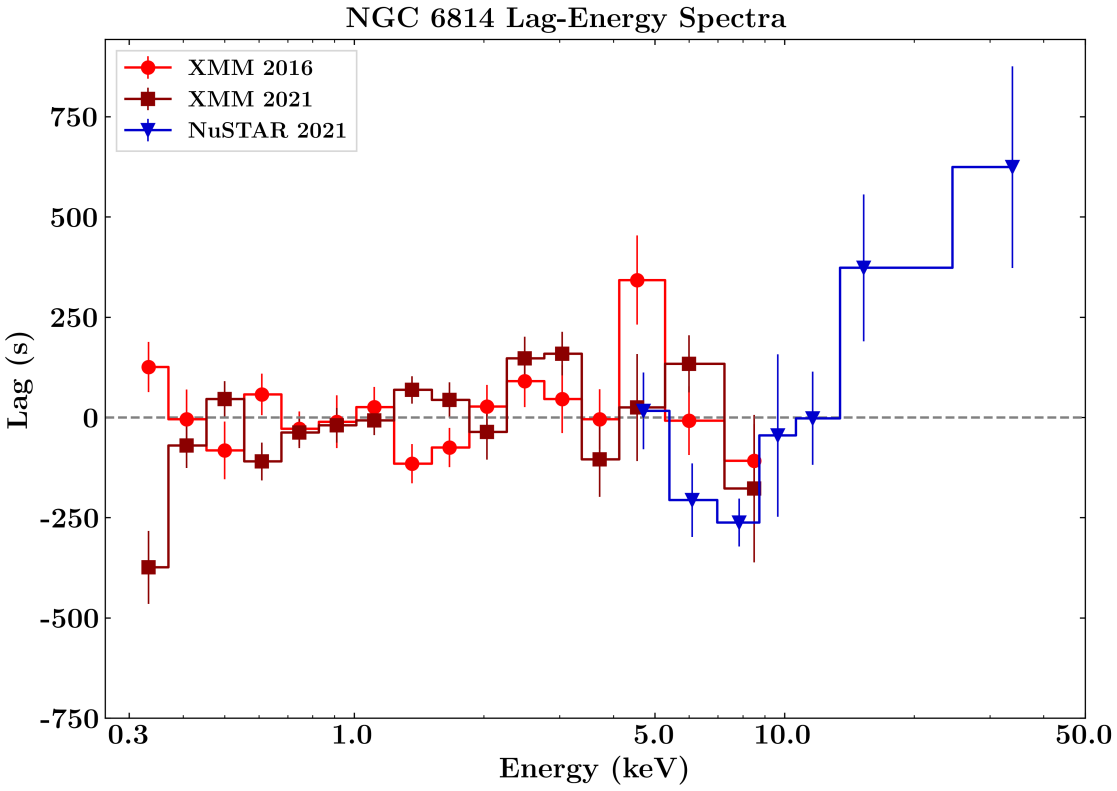

Figure 3.11: Lag-energy spectra measured between $f_{min} = 2 \cdot 10^{-4}$ Hz and $f_{max} = 4 \cdot 10^{-4}$ Hz. As in the lag-frequency spectra, there is no significant lag detected at any energy.

The absence of any lag here is consistent with our lag-frequency result. The shape of the lag-energy spectrum can reveal the spectrum of the lagging component. The spectrum in Fig. 3.11 appears consistent with a power law. This is further evidence that there is no reverberation signal from the reflected emission, either because it is significantly dimmer than the primary emission or because the light travel times between the corona and disc are short.

Chapter 4

Discussion

We have presented a detailed X-ray timing analysis of the Seyfert 1.5 galaxy NGC 6814 using observations from the XMM-Newton and NuSTAR observatories. Through analysis of hardness ratios we found that NGC 6814 follows the "softer when brighter" trend (Fig. 3.3 and Table 3.1), similar to that found by Papadakis et al. (2002) and others. The "softer when brighter" trend was previously thought to occur due to the corona being cooler during bright phases (Kang et al., 2021). But, since this contradicts the "hotter when brighter" trend found by Zhang et al. (2018) and others, it is now thought that corona geometry changes are needed to generate this trend. Specifically, during brighter phases, the corona may be heated to higher temperatures and inflated to a larger size. This would reduce its opacity and lead to a softer spectrum, reproducing both the "softer when brighter" and the "hotter when brighter" trends (Wu et al., 2020).

The hardening during the eclipse in 2016 is consistent with Gallo et al. (2021) and likely a result of the obscurer diminishing the soft X-rays more than at higher energies. Comparing the mean hardness ratios of the observations (Table 3.1) we find that NGC 6814 was in a similar state in 2009 and 2021, with ratios that are close, but not equal, to each other. Both XMM-Newton and NuSTAR observations show that NGC 6814 was in a harder state in 2016 than in 2021. The much steeper

"softer when brighter" trend in the 2016 XMM-Newton observation is in agreement with Kang et al. (2023) which found that this steeper trend is likely dominated by the varying absorption from the obscuring clouds and that the intrinsic flux variability is significantly weaker during the eclipse observation.

Our investigation into the fractional variabilities of each epoch shows that there is a weak decrease in variability with increasing energy which continues into the hard X-rays observed with NuSTAR. This agrees with the hardness ratio curves measured by NuSTAR that show very little spectral variability. The greatest variability occurs in the 2016 XMM-Newton observation which features an eclipse. Here the variability is highest at the low energies, which is again consistent with Gallo et al. (2021) finding that the low-energy X-rays were diminished by 50% by the eclipse, compared to 20% for the high-energies. These measurements support their suggestion that the source size is dependent on energy and that the hard X-rays are emitted from a more compact region in the AGN.

The lack of any significant lag in the lag-frequency spectra suggests there is little to no delay between the soft band (0.3-1 keV for XMM, 4-10 keV for NuSTAR) and hard band (4-10 keV for XMM, 10-50 keV for NuSTAR) in any of the observations we have studied. This is a different result from Walton et al. (2013), which found a hard band lag of ~ 1600 s at low frequencies. This may be because the energy bands they used were 0.5-2 keV and 2-5 keV which is softer than our investigated range. The lack of a reverberation signal implies that either the primary X-ray emission from the corona dominates the reflected emission from the disc, or that the light travel time between the corona and the disc is too short to detect reverberation lags.

The latter would support a proposal by Gonzalez et al. (2024) that the outer disc may be truncated by dust formation. Although they note that some estimates of the minimum radius for dust sublimation to occur (Baskin and Laor, 2018) are too large for outer disc truncation ($r_{dust} \approx 2700\, r_g$), others, such as analysis by Kang et al. (2023) of the clumpy absorber in the 2016 eclipse, place this distance much closer to the central black hole ($r_{dust} \approx 641\, r_g$ or less). These lower estimates would place the outer disc truncation at the edge of the BLR. Such a truncated disc would result in shorter travel times between the corona and disc, and therefore shorter lags between the primary and reflection emission. These short lags (in Fig. 3.11, less than about 250 s) cannot be ruled out in our lag-energy spectra as they are within the uncertainties. Therefore, our analysis would support the scenario of a non-standard accretion disc geometry in NGC 6814.

Chapter 5

Conclusion

In this work, we have used a number of X-ray timing analysis techniques to study the variability of the Seyfert 1.5 galaxy NGC 6814. Our hardness ratio and fractional variability analysis showed that during the 2016 eclipse, the variability in NGC 6814 was dominated by changes in absorption (Sections 3.1, 3.2). However, at all other epochs, including the non-eclipse times in 2016, NGC 6814 behaved as a normal AGN. We found that it follows the "softer when brighter" trend, which likely results from variations in the corona (Section 3.1), that the amplitude of the variations decreases with increasing energy (Section 3.2), and that the variability power increased toward lower frequencies (Section 3.3). In our lag analysis we failed to identify any significant frequency-dependent or energy-dependent lags in either the XMM-Newton or NuSTAR observations. This indicates that the inner-disc blurred reflection component is rather weak in this source and supports suggestions that NGC 6814 may have a non-standard accretion disc.

Future work could include examining other relationships, for example between the excess variance and the brightness, or carrying out Monte Carlo simulations to determine if there are any significant peaks in the power spectra. Our lag analysis could be refined by optimising the energy and frequency bins used to perform the lag analysis, whilst we could test the Gaussian process lag results against more conser-

vative techniques to verify how good this method is at filling in gaps in light curves. Further observations of NGC 6814 would help in all areas of analysis, but there is still plenty to be done with the data we have currently.

Bibliography

Alexei Baskin and Ari Laor. Dust inflated accretion disc as the origin of the broad line region in active galactic nuclei. MNRAS, 474(2):1970–1994, February 2018.

Misty C. Bentz and Sarah Katz. The AGN Black Hole Mass Database. PASP, 127 (947):67, January 2015.

Bradley W. Carroll and Dale A. Ostlie. *An introduction to modern astrophysics, Second Edition*. 2017.

B. De Marco, G. Ponti, M. Cappi, M. Dadina, P. Uttley, E. M. Cackett, A. C. Fabian, and G. Miniutti. Discovery of a relation between black hole mass and soft X-ray time lags in active galactic nuclei. MNRAS, 431(3):2441–2452, May 2013.

A. C. Fabian, A. Zoghbi, R. R. Ross, P. Uttley, L. C. Gallo, W. N. Brandt, A. J. Blustin, T. Boller, M. D. Caballero-Garcia, J. Larsson, J. M. Miller, G. Miniutti, G. Ponti, R. C. Reis, C. S. Reynolds, Y. Tanaka, and A. J. Young. Broad line emission from iron K- and L-shell transitions in the active galaxy 1H0707-495. Nature, 459(7246):540–542, May 2009.

Luigi C. Gallo. Revealing the Innermost Regions of Active Galaxies. JRASC, 105 (4):143, August 2011.

Luigi C. Gallo, Adam G. Gonzalez, and Jon M. Miller. Eclipsing the x-ray emitting region in the active galaxy ngc 6814. *ApJL*, 908(2):L33, 2021.

A. G. Gonzalez, L. C. Gallo, P. Kosec, A. C. Fabian, W. N. Alston, M. Berton, and D. R. Wilkins. Characterizing continuum variability in the radio-loud narrow-line Seyfert 1 galaxy IRAS 17020+4544. MNRAS, 496(3):3708–3724, August 2020.

A. G. Gonzalez, L. C. Gallo, J. M. Miller, E. S. Kammoun, A. Ghosh, and B. A. Pottie. Characterizing X-ray, UV, and optical variability in NGC 6814 using high-cadence Swift observations from a 2022 monitoring campaign. MNRAS, 527(3): 5569–5579, January 2024.

Fiona A. Harrison, William W. Craig, Finn E. Christensen, Charles J. Hailey, William W. Zhang, Steven E. Boggs, Daniel Stern, W. Rick Cook, Karl Forster, Paolo Giommi, Brian W. Grefenstette, Yunjin Kim, Takao Kitaguchi, Jason E. Koglin, Kristin K. Madsen, Peter H. Mao, Hiromasa Miyasaka, Kaya Mori, Matteo Perri, Michael J. Pivovaroff, Simonetta Puccetti, Vikram R. Rana, Niels J. Westergaard, Jason Willis, Andreas Zoglauer, Hongjun An, Matteo Bachetti, Nicolas M. Barrière, Eric C. Bellm, Varun Bhalerao, Nicolai F. Brejnholt, Felix Fuerst,

Carl C. Liebe, Craig B. Markwardt, Melania Nynka, Julia K. Vogel, Dominic J. Walton, Daniel R. Wik, David M. Alexander, Lynn R. Cominsky, Ann E. Hornschemeier, Allan Hornstrup, Victoria M. Kaspi, Greg M. Madejski, Giorgio Matt, Silvano Molendi, David M. Smith, John A. Tomsick, Marco Ajello, David R. Ballantyne, Mislav Baloković, Didier Barret, Franz E. Bauer, Roger D. Blandford, W. Niel Brandt, Laura W. Brenneman, James Chiang, Deepto Chakrabarty, Jerome Chenevez, Andrea Comastri, Francois Dufour, Martin Elvis, Andrew C. Fabian, Duncan Farrah, Chris L. Fryer, Eric V. Gotthelf, Jonathan E. Grindlay, David J. Helfand, Roman Krivonos, David L. Meier, Jon M. Miller, Lorenzo Natalucci, Patrick Ogle, Eran O. Ofek, Andrew Ptak, Stephen P. Reynolds, Jane R. Rigby, Gianpiero Tagliaferri, Stephen E. Thorsett, Ezequiel Treister, and C. Megan Urry. The Nuclear Spectroscopic Telescope Array (NuSTAR) High-energy X-Ray Mission. ApJ, 770 (2):103, June 2013.

Jorge Ernesto Horvath. *High-Energy Astrophysics; A Primer*. 2022.

J. D. Hunter. Matplotlib: A 2d graphics environment. *Computing in Science & Engineering*, 9(3):90–95, 2007.

F. Jansen, D. Lumb, B. Altieri, J. Clavel, M. Ehle, C. Erd, C. Gabriel, M. Guainazzi, P. Gondoin, R. Much, R. Munoz, M. Santos, N. Schartel, D. Texier, and G. Vacanti. XMM-Newton observatory. I. The spacecraft and operations. A&A, 365:L1–L6, January 2001.

Mark H. Jones, Robert J. A. Lambourne, and Stephen Serjeant. *An Introduction to Galaxies and Cosmology*. 2015.

Jia-Lai Kang, Jun-Xian Wang, and Shu-Qi Fu. What can be learnt from a highly informative X-ray occultation event in NGC 6814? A marvellous absorber. MNRAS, 525(2):1941–1952, October 2023.

Jia-Lai Kang, Jun-Xian Wang, and Wen-Yong Kang. Distinct high-energy cutoff variation patterns in two Seyfert galaxies. MNRAS, 502(1):80–88, March 2021.

K. Mukai, C. Hellier, G. Madejski, J. Patterson, and D. R. Skillman. X-Ray Variability of the Magnetic Cataclysmic Variable V1432 Aquilae and the Seyfert Galaxy NGC 6814. ApJ, 597(1):479–493, November 2003.

NASA High Energy Astrophysics Science Archive Research Center (HEASARC). HEAsoft: Unified Release of FTOOLS and XANADU. Astrophysics Source Code Library, record ascl:1408.004, August 2014.

I. E. Papadakis, P. O. Petrucci, L. Maraschi, I. M. McHardy, P. Uttley, and F. Haardt. Long-Term Spectral Variability of Seyfert Galaxies from Rossi X-Ray Timing Explorer Color-Flux Diagrams. ApJ, 573(1):92–104, July 2002.

William Pence and Pan Chai. Fv: Interactive FITS file editor. Astrophysics Source Code Library, record ascl:1205.005, May 2012.

B. Pottie, L. C. Gallo, A. G. Gonzalez, and J. M. Miller. A colourful analysis: Probing the eclipse of the black hole and central engine in NGC 6814 using X-ray colour-colour grids. MNRAS, 525(3):3633–3644, November 2023.

L. Strüder, U. Briel, K. Dennerl, R. Hartmann, E. Kendziorra, N. Meidinger, E. Pfeffermann, C. Reppin, B. Aschenbach, W. Bornemann, H. Bräuninger, W. Burkert, M. Elender, M. Freyberg, F. Haberl, G. Hartner, F. Heuschmann, H. Hippmann, E. Kastelic, S. Kemmer, G. Kettenring, W. Kink, N. Krause, S. Müller, A. Oppitz, W. Pietsch, M. Popp, P. Predehl, A. Read, K. H. Stephan, D. Stötter, J. Trümper, P. Holl, J. Kemmer, H. Soltau, R. Stötter, U. Weber, U. Weichert, C. von Zanthier, D. Carathanassis, G. Lutz, R. H. Richter, P. Solc, H. Böttcher, M. Kuster, R. Staubert, A. Abbey, A. Holland, M. Turner, M. Balasini, G. F. Bignami, N. La Palombara, G. Villa, W. Buttler, F. Gianini, R. Lainé, D. Lumb, and P. Dhez. The European Photon Imaging Camera on XMM-Newton: The pn-CCD camera. A&A, 365:L18–L26, January 2001.

P. Uttley, E. M. Cackett, A. C. Fabian, E. Kara, and D. R. Wilkins. X-ray reverberation around accreting black holes. A&A Rev., 22:72, August 2014.

S. Vaughan, R. Edelson, R. S. Warwick, and P. Uttley. On characterizing the variability properties of X-ray light curves from active galaxies. MNRAS, 345(4): 1271–1284, November 2003.

D. J. Walton, A. Zoghbi, E. M. Cackett, P. Uttley, F. A. Harrison, A. C. Fabian, E. Kara, J. M. Miller, R. C. Reis, and C. S. Reynolds. Hard X-Ray Lags in Active Galactic Nuclei: Testing the Distant Reverberation Hypothesis with NGC 6814. ApJ, 777(2):L23, November 2013.

D. R. Wilkins. Low-frequency X-ray timing with Gaussian processes and reverberation in the radio-loud AGN 3C 120. MNRAS, 489(2):1957–1972, October 2019.

D. R. Wilkins. pylag. https://github.com/wilkinsdr/pyLag, 2022.

Yun-Jing Wu, Jun-Xian Wang, Zhen-Yi Cai, Jia-Lai Kang, Teng Liu, and Zheng Cai. More than softer-when-brighter: The X-ray powerlaw spectral variability in NGC 4051. *Science China Physics, Mechanics, and Astronomy*, 63(12):129512, October 2020.

Ji-Xian Zhang, Jun-Xian Wang, and Fei-Fan Zhu. On Measuring the Variation of High-energy Cutoff in Active Galactic Nuclei. ApJ, 863(1):71, August 2018.

A. Zoghbi, A. C. Fabian, P. Uttley, G. Miniutti, L. C. Gallo, C. S. Reynolds, J. M. Miller, and G. Ponti. Broad iron L line and X-ray reverberation in 1H0707-495. MNRAS, 401(4):2419–2432, February 2010.